nature nanotechnology

SUPPLEMENTARY INFORMATION

DOI: 10.1038/NNANO.2016.168

Iron oxide nanoparticles inhibit tumour growth by inducing pro-inflammatory macrophage polarization in tumour tissues

Saeid Zanganeh, PhD[1,2], Gregor Hutter, MD, PhD[2,3], Ryan Spitler, PhD[1,2], Olga Lenkov, BS[1,2], Morteza Mahmoudi, PhD[4], Aubie Shaw, PhD[5], Jukka Sakari Pajarinen, MD, PhD[6], Hossein Nejadnik, MD, PhD[1,2], Stuart Goodman, MD, PhD[6], Michael Moseley, PhD[1], Lisa M. Coussens, PhD[5], Heike E. Daldrup-Link, MD, PhD[1,2,7,*]

© 2016 Macmillan Publishers Limited, part of Springer Nature. All rights reserved.

DOI: 10.1038/NNANO.2016.168

Supplemental Methods

Iron oxide nanoparticles

The majority of experiments were performed with the ultrasmall superparamagnetic iron oxide (USPIO) nanoparticle compound Ferumoxytol (Feraheme®, AMAG Pharmaceuticals Inc., Cambridge, MA, USA). Ferumoxytol is an FDA-approved iron supplement for intravenous treatment of iron deficiency in patients with impaired renal function [1-5]. Ferumoxytol consists of iron oxide nanoparticles with an iron oxide core and a carboxymethyldextran coating. Ferumoxytol has a mean hydrodynamic diameter of 30 nm, an r1 relaxivity of 15 $s^{-1}mM^{-1}$ and an r2 relaxivity of 89 $s^{-1}mM^{-1}$ at 1.5T and 37°C, 40 Hz [6]. In order to validate findings with an alternate iron oxide nanoparticle compound, additional experiments were performed with Ferumoxtran-10 (Sinerem®, Guerbet, Paris, France), a USPIO compound previously investigated in phase I-III clinical trials for detection of lymph node metastases [7,8], which has recently received approval from regulatory authorities for clinical use in patients in the Netherlands [9]. Ferumotran-10 consists of iron oxide nanoparticles with an iron oxide core and a dextran coating. Ferumoxtran-10 has a hydrodynamic diameter of 15-40 nm, an r1 relaxivity of 22.7 $s^{-1}mM^{-1}$ and an r2 relaxivity of 53 $s^{-1}mM^{-1}$ at 0.47 T and 37 °C, 20 Hz 8. Control experiment was performed with iron-free dextran (FD10S; Sigma-Aldrich, St. Louis, MO).

Transwell Assays

To evaluate, if ferumoxytol nanoparticles have direct chemotactic effects on macrophages, MMTV-PyMT cancer cells and RAW264.7 macrophage cells were co-cultured in dual-chamber transwell systems with 3 μm-sized microporous membranes (Corning, New York, NY, USA), which permits cell translocation between chambers (the 3 μm-sized microporous membrane is recommended by Corning in order to study macrophage migration). Macrophages were pre-labeled with a lipophilic carbocyanine dye, DiD (C67 H103 CIN2 O3 S; 1,19 -dioctadecyl- 3,3,39 ,39 tetramethylindodicarbocyanine, Vybrant® DiD cell-labeling solution, ThermoFisher). Briefly, 1 x 10^6 macrophages were incubated with 5 microliter of DiD dye/mL whole media at 37°C for 20 minutes. The cells were then washed three times with PBS (pH 7.4) by sedimentation (5 minutes, 400 rcf, 25u C). After washing, macrophages were plated onto transwell

© 2016 Macmillan Publishers Limited, part of Springer Nature. All rights reserved.

inserts, MMTV-PyMT cancer cells were seeded into the bottom wells of transwell plates and co-cultures were incubated for 6 hours with ferumoxytol at a concentration of 2.73 mg/mL, which is equivalent to the ferumoxytol dose applied for *in vivo* studies (see below) [10]. All transwell assays were performed with Dulbecco's Modified Eagle's Medium (DMEM), supplemented with 10% fetal bovine serum (FBS) and 1% penicillin/streptomycin. Cells were incubated for 6 hours at 37 °C in a humidified atmosphere with 5% CO_2. Subsequently, the bottom chambers were isolated and cells were stained by 4',6-diamidino-2-phenylindole (DAPI, Invitrogen). DiD positive macrophages that had migrated to the bottom chamber of transwell systems were counted under a Zeiss fluorescence microscope (Zeiss, Oberkochen, Germany), using DAPI and DiD channels and 40x magnification. Control groups were set up without either cancer cells, ferumoxytol or both in the co-culture system. The same volume of phosphate buffered saline (PBS, Gibco, USA) was added instead of ferumoxytol.

To determine M1- and M2-associated gene expression *in vitro,* macrophages from the upper chamber (transwell system with 0.4 µm-sized microporous membranes and 12 h incubation time) were harvested, followed by RNA extraction with the RNeasy mini/micro kit (Qiagen, Valencia, CA, USA) according to the manufacturer's protocol. Cell culture supernatants were also collected and either used directly or stored in -80°C until analyzed. 1 µg of total RNA was reverse-transcribed into complementary DNAs with an iScript complementary cDNA synthesis kit (Bio-Rad, Hercules, CA, USA) containing a mixture of oligo (dT) and random primers. Real-time PCR was performed with primers described previously [11-15] on an ABI PRISM 7900HT Sequence Detection System (Applied Biosystems, Foster City, CA, USA), using a DyNAmo HS SYBR Green qPCR kit (New England BioLabs, Finnzymes, Finland). Cycling conditions were the following: initial denaturation at 95 °C for 10 min, followed by 40 cycles at 95 °C for 15 s and 60 °C for 1 min. mRNA expression levels were determined by the comparative Ct method [16]. To further confirm the production of the M1 marker TNFα and suppression of the M2 marker IL-10, samples were assayed using mouse TNF and IL-10 ELISA kits (Biolegend, San Diego, CA) following the manufacturer's instructions.

© 2016 Macmillan Publishers Limited, part of Springer Nature. All rights reserved.

DOI: 10.1038/NNANO.2016.168

To evaluate production of reactive oxygen species (ROS) by cells in the transwell system, RAW264.7 macrophages were co-cultured with MMTV-PyMT cancer cells in transwell plates with 0.4 μm pore-size (12-well, Corning), which allowed free diffusion of molecules between the two chambers but not cell translocation. Since RAW264.7 macrophages are isolated from the BALB/c mouse, which is derived from a different strain than the MMTV-PyMT tumour (FVB/N), we confirmed our results using autologous bone marrow-derived macrophages isolated from FVB/N mice, as described previously [17]. Briefly, mice were euthanized, bilateral femurs and tibias were explanted, bone marrow cavities were flushed with DMEM supplemented with 10% FBS and 5 ng/mL macrophage colony-stimulating factors (M-CSF, PeproTech, Rocky Hill, NJ, USA), bone marrow cells were pipetted into single-cell suspension and incubated at 37°C for 2 h before plating. 0.7 x10^6 cells were seeded to one insert of a 6-well transwell plate. 5 days later, cancer cells were seeded to the bottom chamber of the transwell plate (0.4 μm, Corning), with or without addition of ferumoxytol at a concentration of 2.73 mg/mL, followed by caspase activity detection on the next day. Active caspase-3 detection in cancer cells was performed by immunocytochemistry. Cells were blocked in PBS containing 1.5% Bovine Serum Albumin (BSA, Sigma Aldrich, St Louis, MO, USA) and 3% Normal Goat Serum (Cell Signaling Technology Inc, Beverly, MA, USA) for 1 h. Cells were then stained against Human/Mouse Active Caspase-3 Antibody (R&D System, Minneapolis, MN, USA) at 1:100 dilutions in PBS supplemented with 0.5% BSA. Counterstains of intracellular actins and nuclei were performed by incubating the cell samples for 1 h with Rhodamine-Phalloidin (Invitrogen, Eugene, OR, USA) at 1:200 dilutions in 0.5% BSA containing PBS solution and fixed with a DAPI mounting solution (Invitrogen).

Culture media was retrieved from co-cultures described above and ROS levels were measured using two different ROS indicators: The hydroxyl radical was measured by incubating co-culture media with 3'-(p-hydroxyphenyl) fluorescein (HPF; ThermoFisher Scientific, Waltham, MA Cat# H36004) at a concentration of 10 mM for 30 min at 37°C and measuring HPF fluorescence at an emission wavelength of 515 nm (excitation wavelength 490 nm). In addition, hydrogen peroxide in co-culture media was measured by incubating co-culture media with a hydrogen peroxide colorimetric detection kit for 30 min

© 2016 Macmillan Publishers Limited, part of Springer Nature. All rights reserved.

at 25°C (Enzo Life Science, Farmingdale, NY; Cat# ADI907015) and measuring the resultant absorbance at 550 nm. Control groups included cancer cells, ferumoxytol, macrophages or any combination in a co-culture system. To understand the effect of caspase expression on ROS production, control experiments were performed after administration of Z-DEVD-FMK (caspase-3 inhibitor, 100 μM, R&D Systems, Inc, USA). Cancer cells were first pretreated for 1 h with Z-DEVD-FMK and then the residual Z-DEVD-FMK was washed three times with cold PBS before cancer cells were co-cultured with macrophages in the transwell system.

Small animal MRI

We implanted 2.3 x 10^6 MMTV-PyMT-derived cancer cells into the bilateral mammary fat pads of female FVB/N mice, with or without addition of ferumoxytol (2.73 mg Fe/mL). All mice underwent magnetic resonance (MR) imaging under isofluorane anesthesia (n=7 mice, experimental group 1), using a 7 Tesla animal MR scanner (General Electric-Varian "microSigna 7.0"), a 45 mm Millipede radiofrequency coil (Varian Inc., Palo Alto, CA, USA) and a T2*-weighted 2D fast gradient echo (FGRE) pulse sequence with a flip angle of 20°, a repetition time of 70 ms, multiple echo times of 1.5-12.6 ms (8 echoes with echo spacing of 1.6 ms), a matrix of 128x128 pixels, a field of view of 4.5x2.7 cm, one excitation and a slice thickness of 0.6 mm. T2* relaxation time maps were generated from multi-echo FGRE images by fitting the relaxation equation $M(TE)^2\_ = M^20 \exp(-2TE/T2^*)$ to the image data, using a custom research software (Cinetool,GE Global Research Center). T2* relaxation times, which are proportional to local iron concentrations, were measured on T2* relaxation time maps and compared between iron-co-injected and control implantation sites, using a t-test.

Tumour model of liver and lung metastases

Liver tumours were induced in NOD.Cg-*Prkdc*^{scid} *Il2rg*^{tm1Wjl}/SzJ mice by intravenous injection of 1×10^4 or 2×10^4 small cell lung cancer cells[7,18] (SCLC, KP1-GFP-Luc). KP1-GFP-Luc cells were grown in RPMI media containing 10% Fetal bovine growth serum (Fisher Scientific) at 5% CO_2 and 37°C. Cells were washed with PBS before use, diluted in 0.5 ml of saline and injected via the tail vein. The tumour cells are

© 2016 Macmillan Publishers Limited, part of Springer Nature. All rights reserved.

DOI: 10.1038/NNANO.2016.168

small enough that many can pass the pulmonary capillary bed, thereby leading to liver and pulmonary metastases[18].

Tissue dissociation and flow cytometry

Mice were euthanized with Ketamine (100mg/kg) and Xylazine (10 mg/kg) intraperitoneally followed by transcardial perfusion with ice-cold PBS. All tumour, liver and lung samples were divided in two pieces, weighted and processed for both flow cytometry and histopathology. Tumour, liver and lung samples were taken into ice-cold PBS, minced with a razor blade, washed and incubated for 30 min at 37 °C in DMEM (Invitrogen) with 2.0 mg/mL Collagenase A (Roche, Basel, Switzerland) and 50 units/mL DNase I (Roche, Basel, Switzerland). Single cell suspensions were prepared by filtering through 70-µm nylon strainers (BD Biosciences). Cells were washed, and in the case of liver samples, ACK-lysis (Gibco Life Technologies, Carlsbad, CA, USA) was performed. Thereafter, cells were incubated for 15 min on ice with Fc Receptor Binding Inhibitor (eBioscience, USA) diluted 1/10 in PBS containing Zombie-Aqua fixable viability stain (BioLegend, San Diego, CA, USA) to exclude dead cells. Cells were then incubated for 30 min in PBS containing 1.0 mM EDTA and 5% FCS along with manufacturers' suggested dilutions of fluorescently labeled primary monoclonal antibodies. The following antibodies were used for analysis of liver and lung macrophages: anti-CD11b-PerCP-Cy5.5, anti-Ly6G-PE anti-F4/80-Alexa Fluor 700, anti-CD80-Alexa Fluor 647, CD206 PE-Cy7, Anti-CD45-Pacific Blue, Zombie-Aqua fixable viability stain (all BioLegend, San Diego, CA, USA) stain was added to exclude dead cells. The antibodies were used for analysis of breast tumour macrophages are listed in Supplementary Table 1. Acquisition was performed on an LSRII Fortessa flow cytometer (BD-Biosciences, New Jersey, USA). Data analysis was performed using FlowJo Version 9.6.4 (Tree Star). Live singlets were gated using FSC-W/FSC-H (Supplementary Figure 5a). Liver macrophages were identified as $CD45^{+}Ly6C^{-}CD11c^{-}CD11b^{+}$ cells (Supplementary Figure 5b). Liver tissue-resident macrophages were defined as $F4/80^{high}$ $CD11b^{low}$, whereas infiltrating macrophages were $CD11b^{high}$ $F4/80^{low}$. Lung macrophage/dendritic cell subsets were identified as described in **Fig. 4b**.

© 2016 Macmillan Publishers Limited, part of Springer Nature. All rights reserved.

Histology

Tumour samples were embedded in Tissue-Tek OCT compound, snap frozen in liquid nitrogen and cut into 8 µm thick frozen sections using a cryostat. Sections were fixed in ice-cold acetone for 10 min at -20°C followed by two 5 min washes in phosphate buffered saline (PBS) and 1 hour blocking in 1% bovine serum albumin (BSA)-PBS. Antibodies against CD206 (2 µg/mL, PE-conjugated, monoclonal rat anti-mouse IgG2a κ; BioLegend, San Diego, CA), CD80 (4 µg/mL, Alexa Fluor 488-conjugated Armenian Hamster anti-mouse IgG, BioLegend, San Diego, CA), CD11b (4 µg/mL, FITC-conjugated rat anti-mouse IgG2b κ, BD), and the corresponding isotype controls were diluted in 1% BSA-PBS to the indicated concentrations and then applied to the sections followed by overnight incubation at 4°C in the dark. Sections were washed three times with PBS for 5 min and mounted with ProLong Glod with DAPI (Life Technologies, Pleasanton, CA), imaged with 40X magnification with an Axio Zeiss microscope (Axio Observer 3.1; Zeiss, Oberkochen, Germany) and the resultant digital images were analyzed using the ImageJ (National Institute of Health). Cell nuclei, CD80 and CD206 positive cells were counted by ImageJ based on the method described by Papadopulos and co-workers [19].Student's t-test was used to determine differences between early and last stage tumour groups, considering $p < 0.05$ as statistically significant.

Prussian blue stain was used as part of the Accustain Iron Stain Kit (Sigma-Aldrich, St. Louis, MO, USA) to qualitatively assess the iron uptake of liver samples of hepatic metastasis. Liver tissues were embedded in Tissue-Tek OCT compound, snap frozen in liquid nitrogen and sectioned into 8 µm thick slices using a cryostat. The slides were then fixed in a neutral buffered formalin solution, incubated for 15 minutes in a 1:1 solution of Potassium Ferrocyanide and Hydrochloric Acid and then incubated with 3,3'-Diaminobenzidine (DAB) for 3 minutes. The slides were rinsed once and then stained with a 1:50 dilution of Fast Nuclear Red solution in deionized water. After the final rinse, the sample was dehydrated using serial concentrations of ethanol, mounted and imaged for the presence or absence of positive blue iron staining.

© 2016 Macmillan Publishers Limited, part of Springer Nature. All rights reserved.

DOI: 10.1038/NNANO.2016.168

Supplemental Figure Legends

Supplementary Figure 1. Low dose ferumoxytol was not cytotoxic.

Caspase 3/7 activity of different cell types after co-incubation with ferumoxytol for 24 hours at different iron concentrations. Up to a concentration of 3 mg/mL, which is equivalent to the applied concentration for *in vivo* experiments (2.73 mg/mL), ferumoxytol did not reveal cytotoxic effects on cancer cells. Further increase of ferumoxytol concentrations ranging from 3 to 30 mg/mL induced a dose-dependent cytotoxicity on all indicated cell lines. Data are displayed as the means of 3 independent experiments per experimental group plus standard deviation. * Indicates statistical significance ($p < 0.05$, Student's t-test,) in comparison with control cells treated with PBS.

Supplementary Figure 2. Ferumoxytol increased macrophage migration.

a, Diagram shows macrophage-cancer cell co-culture set up in transwell plates (3 µm-sized microporous membrane allows for migration of macrophages). DiD-labeled macrophages were seeded onto the insert and cancer cells were seeded onto the bottom chamber. 2.73 mg/mL Ferumoxytol was added to the culture medium. Macrophage migration was analyzed 6 hours later after counterstaining cells in the lower chamber with DAPI. **b**, Representative images were taken by a Leica fluorescence microscope at a magnification of 10 x (Scale bar = 150 µm) and show increased migration of red fluorescent macrophages to bottom chambers that contained cancer cells and ferumoxytol compared to cancer cells or ferumoxytol alone. **c**, Corresponding quantitative data show significantly increased macrophage migration to cancer cell – ferumoxytol co-cultures. Macrophage counts were averaged from 15-20 fields of view using a fluorescence microscope at 40X. Data were collected from at least 3 independent experiments in triplicate. * Indicates statistical significance ($p < 0.05$, Student's t-test, Error bars represent the mean ± standard deviations) between macrophages stimulated by both ferumoxytol and cancer cells, compared with cells incubated with ferumoxytol or cancer cells individually.

© 2016 Macmillan Publishers Limited, part of Springer Nature. All rights reserved.

Supplementary Figure 3. Ferumoxytol can inhibit tumour growth

To evaluate whether ferumoxytol treatment could completely suppress tumour growth, we implanted decreasing numbers of 2.3, 1, 0.1 and 0.01 x 10^6 MMTV PyMT cancer cells into the bilateral mammary fat pad, with or without ferumoxytol. **a**, Representative whole body fluorescence imaging at 21 days post-inoculation show overall suppressed tumour growth in the presence of ferumoxytol and maximum tumour suppression for the lowest cancer cell load. **b**, Corresponding tumour volumes were significantly lower for ferumoxytol co-implanted tumours compared to untreated controls ($P< 0.05$, ANOVA, Data displayed as the mean of seven tumours per group ± standard deviations). Maximum tumour growth inhibition was noted for 0.01 x 10^6 co-implanted cells. **c**, Representative immunofluorescence stains at day 21 after implantation of 0.01 x 10^6 MMTV PyMT cancer cells into the bilateral mammary fat pad, with or without ferumoxytol. Ferumoxytol co-implanted tumours contain increased $CD80^+$ M1 populations (green) and decreased $CD206^+$ M2 populations (red) compared to cancer cells only. (Scale bar = 100 μm) **d**, The number of positive cells in 10 high power fields on each stain were counted and quantified for 7 sections per tumour. Ferumoxytol co-implanted tumours showed significantly increased $CD80^+$ M1 populations compared to controls. Data represent the mean of 7 tumours per group ± standard deviations. ($P< 0.05$) indicates a statistically significant difference (Student's t-test) from cancer cell injected control.

Supplementary Figure 4. α-CSF1 monoclonal antibody treatment inhibits ferumoxytol effects on tumour **growth**

Mice were co-implanted with MMTV-PyMT tumours, with and without ferumoxytol, and treated with anti-colony stimulating factor monoclonal antibody (α-CSF1 mAb), which depletes TAMs, and/or IgG.

a, Serial tumour volume measurements up to day 21 after tumour cell inoculation. **b,** Immunofluorescence stains for CD11b, (red) and DAPI (blue) of tumour sections obtained at 21 days post implantation of cancer cells with and without ferumoxytol and/or α-CSF1 mAb treatment. (Scale bar = 50 μm). **c**, The number of CD11b positive cells in 10 high power fields were counted and quantified for 7 immunofluorescence images (7 biological replicates per group) for each stain respectively. * and **

© 2016 Macmillan Publishers Limited, part of Springer Nature. All rights reserved.

DOI: 10.1038/NNANO.2016.168

Indicate significant difference ($p < 0.05$, Student's t-test, Error bars represent the mean ± standard deviations) compared to non α-CSF1 monoclonal antibody treated controls.

Supplementary Figure 5. Gating tree for liver macrophage assessment.

a, Flow cytometry gating tree to assess hepatic macrophage subsets used for polarization analysis. **b**, Tumour load assessment in control and ferumoxytol treated mice (n=7 per group). Tumour cells are $GFP^{+}CD45^{-}$. Cf. graphical representation in Fig. 6d.

Supplemental References

1 Balakrishnan, V. S. *et al.* Physicochemical properties of ferumoxytol, a new intravenous iron preparation. *Eur J Clin Invest* **39**, 489-496, doi:ECI2130 [pii] 10.1111/j.1365-2362.2009.02130.x (2009).

2 Landry, R., Jacobs, P. M., Davis, R., Shenouda, M. & Bolton, W. K. Pharmacokinetic study of ferumoxytol: a new iron replacement therapy in normal subjects and hemodialysis patients. *Am J Nephrol* **25**, 400-410, doi:AJN2005025004400 [pii] 10.1159/000087212 (2005).

3 Lu, M., Cohen, M. H., Rieves, D. & Pazdur, R. FDA report: Ferumoxytol for intravenous iron therapy in adult patients with chronic kidney disease. *Am J Hematol* **85**, 315-319, doi:10.1002/ajh.21656 (2010).

4 Neuwelt, E. A. *et al.* The potential of ferumoxytol nanoparticle magnetic resonance imaging, perfusion, and angiography in central nervous system malignancy: a pilot study. *Neurosurgery* **60**, 601-611; discussion 611-602, doi:10.1227/01.NEU.0000255350.71700.3700006123-200704000-00005 [pii] (2007).

5 Pai, A. B., Nielsen, J. C., Kausz, A., Miller, P. & Owen, J. S. Plasma pharmacokinetics of two consecutive doses of ferumoxytol in healthy subjects. *Clin Pharmacol Ther* **88**, 237-242, doi:clpt201080 [pii] 10.1038/clpt.2010.80 (2010).

6 Corot, C., Robert, P., Idee, J. M. & Port, M. Recent advances in iron oxide nanocrystal technology for medical imaging. *Advanced drug delivery reviews* **58**, 1471-1504, doi:10.1016/j.addr.2006.09.013 (2006).

7 Anzai, Y. *et al.* Evaluation of neck and body metastases to nodes with ferumoxtran 10-enhanced MR imaging: phase III safety and efficacy study. *Radiology* **228**, 777-788, doi:10.1148/radiol.2283020872 (2003).

8 Ralph Weissleder, B. D. R., Alnawaz Rehemtulla, Sanjiv Sam Gambhir. *Molecular Imaging: Principles and Practice*(PMPH-USA, 2010).

9 Fortuin, A. S., Meijer, H., Thompson, L. C., Witjes, J. A. & Barentsz, J. O. Ferumoxtran-10 ultrasmall superparamagnetic iron oxide-enhanced diffusion-weighted imaging magnetic resonance imaging for detection of metastases in normal-sized lymph nodes in patients with bladder and prostate cancer: do we enter the era after extended pelvic lymph node dissection? *European urology* **64**, 961-963; discussion 963, doi:10.1016/j.eururo.2013.08.017 (2013).

© 2016 Macmillan Publishers Limited, part of Springer Nature. All rights reserved.

10 Ittrich, H., Peldschus, K., Raabe, N., Kaul, M. & Adam, G. Superparamagnetic iron oxide nanoparticles in biomedicine: applications and developments in diagnostics and therapy. *RoFo : Fortschritte auf dem Gebiete der Rontgenstrahlen und der Nuklearmedizin* **185**, 1149-1166, doi:10.1055/s-0033-1335438 (2013).

11 Hughes, J. E. *et al.* Sphingosine-1-phosphate induces an antiinflammatory phenotype in macrophages. *Circulation research* **102**, 950-958, doi:10.1161/CIRCRESAHA.107.170779 (2008).

12 Kigerl, K. A. *et al.* Identification of two distinct macrophage subsets with divergent effects causing either neurotoxicity or regeneration in the injured mouse spinal cord. *The Journal of neuroscience : the official journal of the Society for Neuroscience* **29**, 13435-13444, doi:10.1523/JNEUROSCI.3257-09.2009 (2009).

13 Scarfi, S. *et al.* Ascorbic acid pre-treated quartz stimulates TNF-alpha release in RAW 264.7 murine macrophages through ROS production and membrane lipid peroxidation. *Respiratory research* **10**, 25, doi:10.1186/1465-9921-10-25 (2009).

14 Villalta, S. A. *et al.* Interleukin-10 reduces the pathology of mdx muscular dystrophy by deactivating M1 macrophages and modulating macrophage phenotype. *Human molecular genetics* **20**, 790-805, doi:10.1093/hmg/ddq523 (2011).

15 Wang, H. *et al.* Histone deacetylase inhibitor LAQ824 augments inflammatory responses in macrophages through transcriptional regulation of IL-10. *Journal of immunology* **186**, 3986-3996, doi:10.4049/jimmunol.1001101 (2011).

16 Shi, Q. *et al.* A combinatorial approach for targeted delivery using small molecules and reversible masking to bypass nonspecific uptake in vivo. *Gene therapy* **17**, 1085-1097, doi:10.1038/gt.2010.55 (2010).

17 Weischenfeldt, J. & Porse, B. Bone Marrow-Derived Macrophages (BMM): Isolation and Applications. *CSH protocols* **2008**, pdb prot5080, doi:10.1101/pdb.prot5080 (2008).

18 Jahchan, N. S. *et al.* A drug repositioning approach identifies tricyclic antidepressants as inhibitors of small cell lung cancer and other neuroendocrine tumors. *Cancer discovery* **3**, 1364-1377, doi:10.1158/2159-8290.CD-13-0183 (2013).

19 Hadjipanayis, C. G. *et al.* EGFRvIII antibody-conjugated iron oxide nanoparticles for magnetic resonance imaging-guided convection-enhanced delivery and targeted therapy of glioblastoma. *Cancer research* **70**, 6303-6312, doi:10.1158/0008-5472.CAN-10-1022 (2010).

© 2016 Macmillan Publishers Limited, part of Springer Nature. All rights reserved.

DOI: 10.1038/NNANO.2016.168

Supplementary Figure 1.

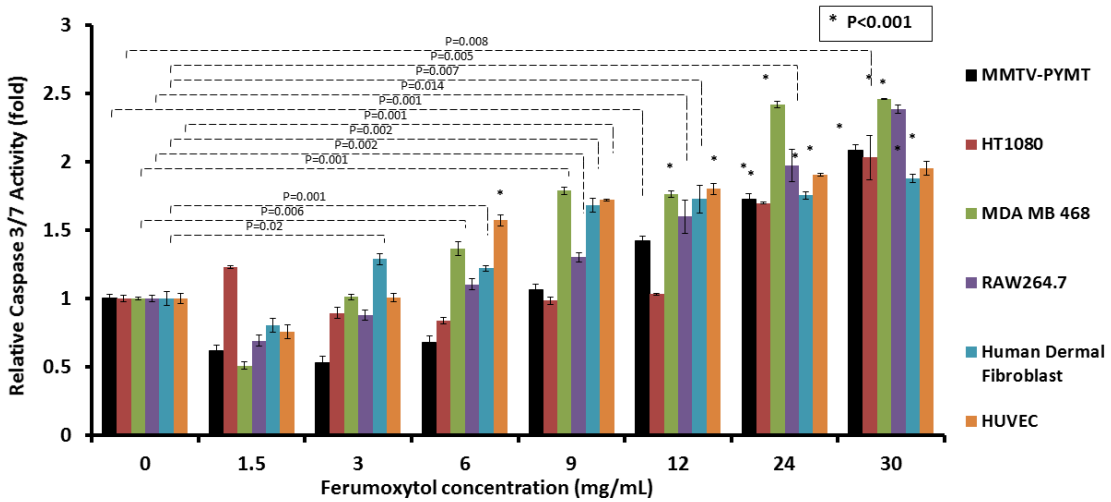

© 2016 Macmillan Publishers Limited, part of Springer Nature. All rights reserved.

Supplementary Figure 2.

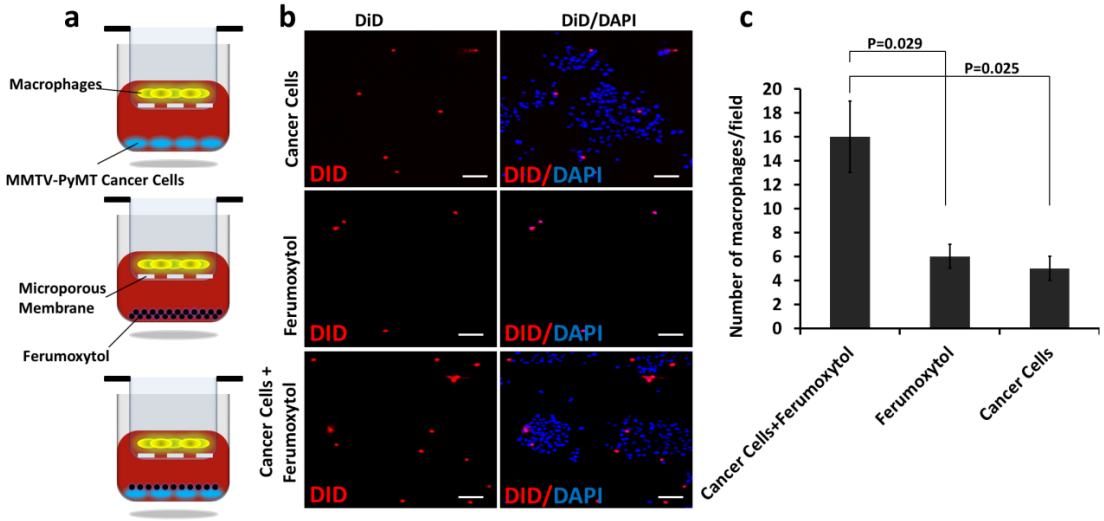

© 2016 Macmillan Publishers Limited, part of Springer Nature. All rights reserved.

DOI: 10.1038/NNANO.2016.168

Supplementary Figure 3.

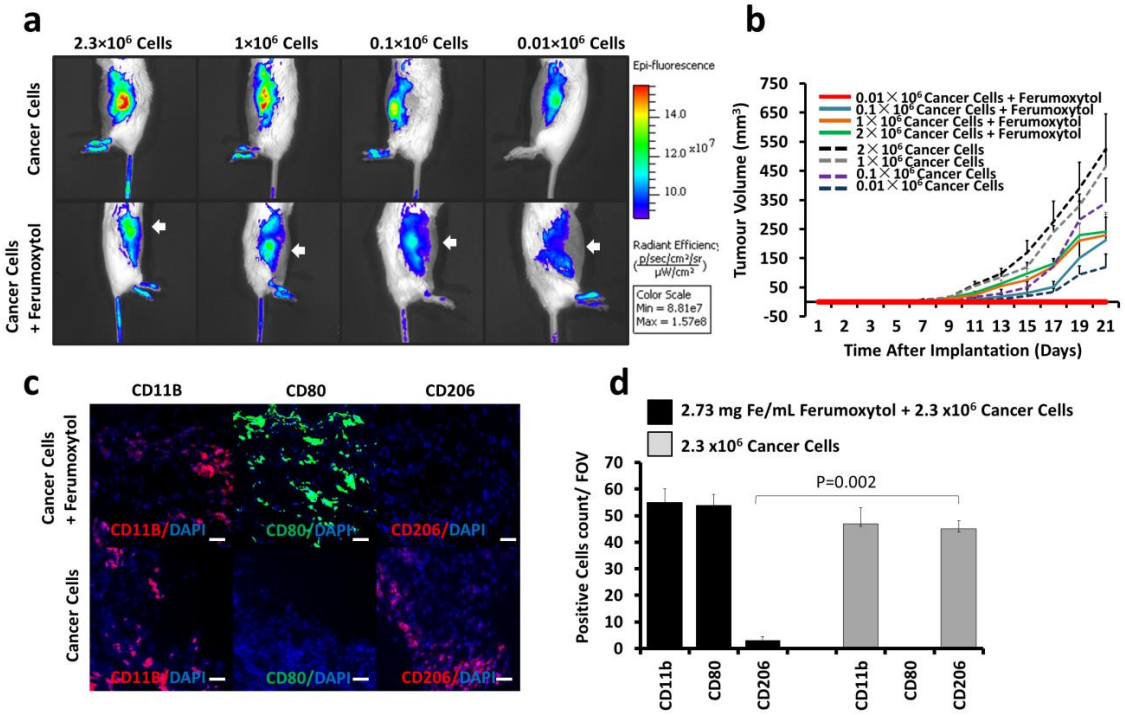

© 2016 Macmillan Publishers Limited, part of Springer Nature. All rights reserved.

Supplementary Figure 4.

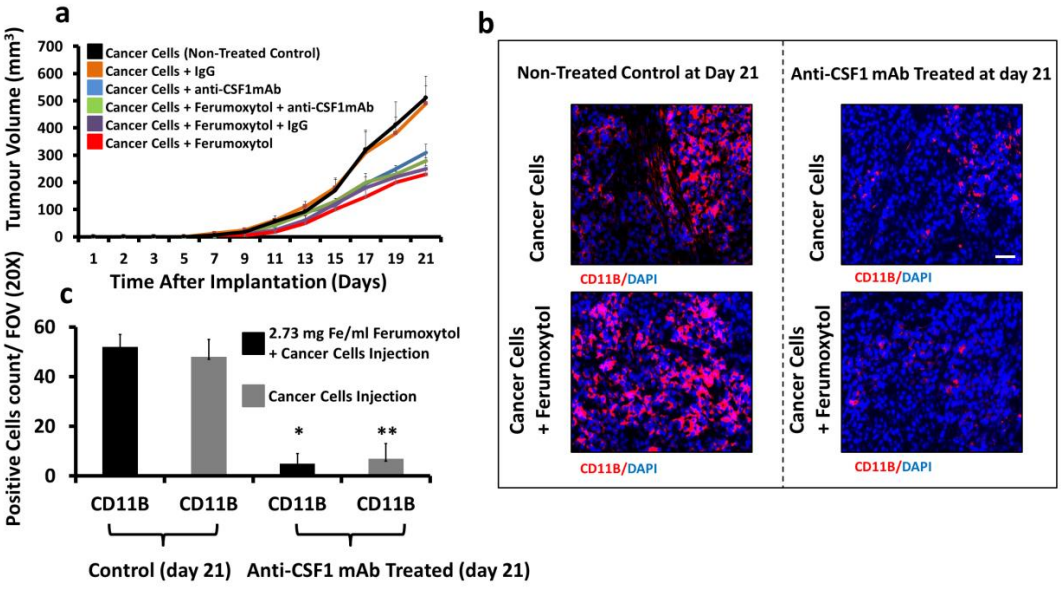

© 2016 Macmillan Publishers Limited, part of Springer Nature. All rights reserved.

DOI: 10.1038/NNANO.2016.168

Supplementary Figure 5.

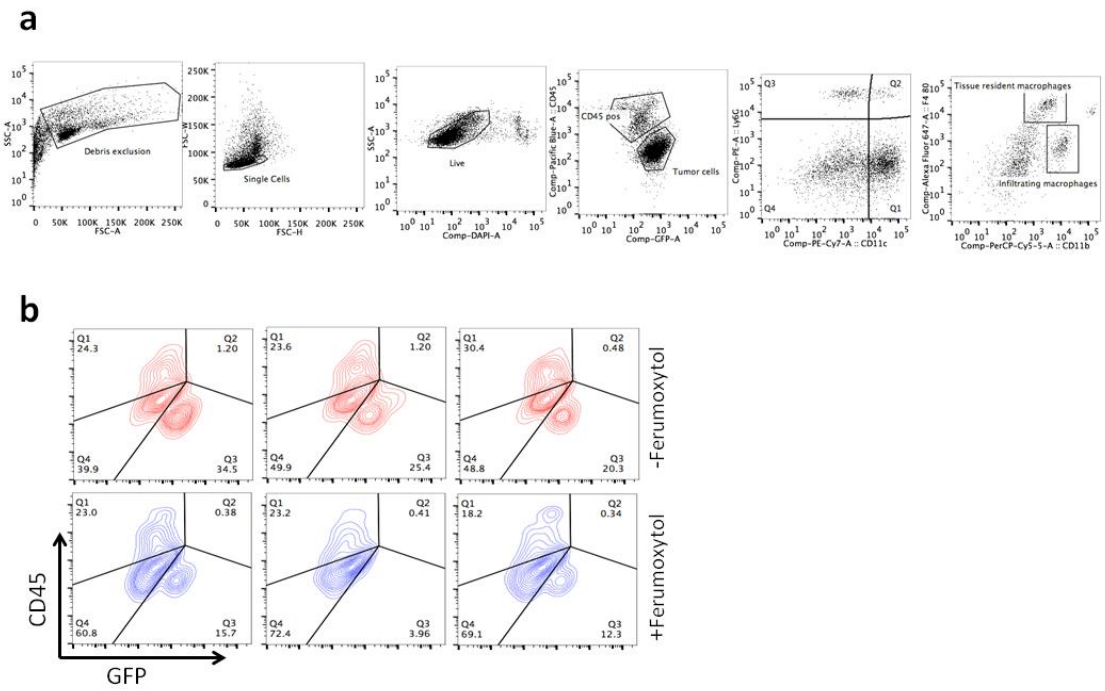

© 2016 Macmillan Publishers Limited, part of Springer Nature. All rights reserved.

Supplementary Table 1. Antibodies used for flow cytometry

Antigen	Clone	Fluorophore	Company	Catalog no.
CD11c	N418	PE/Cy7	BioLegend	117317
CD80	16-10A1	Alexa Fluor® 647	BioLegend	104718
F4/80	BM8	APC	BioLegend	123115
F4/80	BM8	Alexa Fluor® 700	BioLegend	123130
CD11b	M1/70	Alexa Fluor® 647	BioLegend	101218
CD11b	M1/70	PerCP/Cy5.5	BioLegend	101227
Ly6C	eBioscience	PerCP Cy5.5-	eBioscience	45-5932-80
Ly-6C	HK1.4	FITC	BioLegend	128005
CD45	30-F11	Pacific Blue™	BioLegend	103126
CD45	30-F11	PE-Cy7	BioLegend	103114
CD206 (MMR)	C068C2	PE	BioLegend	141706
CD206 (MMR)	C068C2	PE-Cy7	BioLegend	141719
CD3	OKT3	PerCP-eFluor 710	eBioscience	46-0037-42
CD3	OKT3	PerCP-Cy5.5	eBioscience	45-0037-42
CD19	HIB19	Alexa 700	eBioscience	56-0199-73
CD19	HIB19	PerCP-Cy5.5	eBioscience	45-0199-73
MHCII	M5/114.15.2	Alexa 700	eBioscience	56-5321-82
CD49b	DX5	PE	eBioscience	14-5971-85
Ly-6G	RB6-8C5	FITC	eBioscience	14-5931-86
Ly-6C	HK1.4	APC	eBioscience	17-5932-82
TCR	IP26	FITC	eBioscience	11-9986-42
CD4	RPA-T4	Qdot 655	Invitrogen	Q10007
CD4	RPA-T4	PE	BioLegend	300508
CD8	RPA-T8	APC-eFluor 780	eBioscience	47-0088-42
CD8	RPA-T8	Qdot 605	Invitrogen	Q10009

© 2016 Macmillan Publishers Limited, part of Springer Nature. All rights reserved.